06 Aug 2014

In Vitro Assessment of Laser Sintered Bioactive Glass Scaffolds with Different Pore Geometries

Krishna C. R. Kolan

Albin Thomas

Ming-Chuan Leu
Missouri University of Science and Technology, mleu@mst.edu

Greg Hilmas
Missouri University of Science and Technology, ghilmas@mst.edu

In Vitro Assessment of Laser Sintered Bioactive Glass Scaffolds with Different Pore Geometries

Krishna C. R. Kolan[1], Albin Thomas[1], Ming C. Leu[1], and Gregory E. Hilmas[2]

[1]Department of Mechanical and Aerospace Engineering, Missouri University of Science and Technology, Rolla, MO 65409
[2]Department of Materials Science and Engineering, Missouri University of Science and Technology, Rolla, MO 65409

REVIEWED

Abstract

The pore geometry of bioactive glass scaffolds intended for use in bone repair or replacement is one of the most important parameters that could determine the rate of bone regeneration. The pore geometry would also affect the mechanical properties of the scaffolds and their rate of degradation. Scaffolds with five different architectures, having ~50% porosity, were fabricated with silicate (13–93) and borate (13–93B3) based bioactive glasses using a laser sintering process. An established, late-osteoblasts/early-osteocytes cell line was used to perform cell proliferation tests on the scaffolds. The results indicated that the cells proliferate significantly more on the scaffolds which mimic the trabecular bone architecture compared to traditional lattice structures.

1. Introduction

The discovery of Bioglass® by Prof. Hench in 1969 has led to active research interest in the field of bioactive materials in the past four decades [1, 2]. The Bioglass® is a commercially available bioactive glass containing mainly SiO_2, Na_2O, and CaO. Over the years, other beneficial elements were added to the base ternary system and the weight percentage of the elements has changed to develop new glasses which offer excellent bioactive characteristics compared to glass-ceramics or ceramics [3]. 13-93 glass is a silicate based bioactive glass which is FDA approved and has a relatively high SiO_2 content compared to 45S5 glass. Although the rate of degradation slows down due to the higher SiO_2 content, 13-93 glass has been shown to have superior mechanical properties, promote growth and differentiation of osteoblasts *in vitro* and bone growth *in vivo* for repair of a critical size bone [4-6]. The molar concentration of SiO_2 in 13-93 glass has also been replaced by B_2O_3 in the 13-93B3 glass formulation. Borate based glasses are chemically less durable than silicate based glasses, and therefore degrade at a faster rate and allows faster bone formation [7]. Borate based bioactive glasses not only bond to the surrounding hard tissue but are also known to bond with soft tissues [7]. Table 1 shows the compositions of the borate based 13-93B3 bioactive glass versus the silicate based 13-93 bioactive glass. The original Bioglass® formulation by Prof. Hench, termed 45S5 glass, is also presented for comparison.

Table 1. Compositions (in wt.%) of 13-93 and 13-93B3 glasses compared to 45S5 glass.

	SiO_2	P_2O_5	CaO	MgO	Na_2O	K_2O	B_2O_3
45S5	45	6	24.5	-	24.5	-	-
13-93	53	4	20	5	6	12	-
13-93B3	-	3.7	18.5	4.6	5.5	11.1	56.6

Porosity, pore size, and pore geometry are some of the important aspects of a scaffold for bone repair and they affect material degradation and mechanical properties. Although porosity and pore size can be controlled using the extrusion based additive manufacturing (AM) processes like the Freeze-form Extrusion Fabrication [8] and Robocasting [9-11] processes, these processes provide very limited control over the pore geometry in fabricating porous parts because of the layer-by-layer filament deposition in the fabrication process. In comparison, powder-bed based AM techniques like the selective laser sintering (SLS) or selective laser melting (SLM) processes provide flexibility in fabricating porous parts with complex pore geometries and lattice structures as they do not require support structures during part fabrication, which allows for better control of part geometry at a microstructural level (10's of microns). In our previous work, we have shown that 13-93 glass scaffolds fabricated by the SLS process provide good mechanical properties and preferable surface morphology for cell proliferation [12, 13]. Our investigation on the effects of pore geometry on the mechanical properties of the scaffolds, and their degradation behavior when immersed in simulated body fluid, suggested that pore geometry significantly affects the scaffold's mechanical properties at lower porosities compared to at higher porosities [14]. The technical literature contains only limited studies on the effect of pore geometry on cell proliferation. Some of the studies indicate that the cells react to the local curvature of the pore and the permeability of the implant *in vivo* [15, 16]. Additionally, more recent studies have indicated that complex pore geometry for the scaffold aids in achieving good cell seeding efficiency [17, 18]. Overall, it is still unclear to the scientific community as to how pore geometry affects tissue growth. Therefore, AM processes provide an opportunity to investigate the effects of scaffold pore geometry *in vitro*.

In the current work, we investigated the effects of pore geometry in the bioactive glass scaffolds on cell proliferation in a static cell culture. Scaffolds made with 13-93 glass and 13-93B3 glasses were fabricated with ~50% porosity using five different pore geometries. The fabricated scaffolds were seeded with bone cells and incubated at ~37°C for 2, 4, and 6 days followed by MTT assays to quantify the metabolically active cells. Section 2 describes the materials and methods used for this study. Section 3 presents and discusses the cell proliferation results obtained for the 13-93 and 13-93B3 scaffolds.

2. Materials and Methods

2.1. Fabrication of scaffolds

13-93 and 13-93B3 bioactive glasses (prepared by Mo-Sci Corp., Rolla, MO) with an average particle size of 12 μm (d_{50} – 50% of the particles are less than 12 μm) and d_{90} of 30 μm were used in this research. Particle size distributions were obtained using a laser diffraction-based particle size analyzer (S3500, Microtrac Inc., Largo, FL). The glass particles were mixed with stearic acid as the sole binder ($C_{18}H_{36}O_2$, grade HS, Acros Organics, Morris Plains, NJ) and dry ball-milled for 8 hrs with ZrO_2 milling media to obtain the feedstock powder for the SLS machine. A binder content of 15% by weight was used for this purpose as this quantity provides the best possible results and is based on our previous study of SLS using 13-93 bioactive glass [19]. The fabrication experiments were carried out on a commercial DTM Sinterstation 2000 machine. The effect of SLS parameters on fabricating scaffolds using stearic acid binder and bioglass powder has been investigated in our previous work. The same set of parameters (laser

power – 5 W, scan speed – 508 mm/s, scan spacing – 0.23 mm, layer thickness – 0.076 mm) were adopted for the current study [19]. The fabricated green parts were post-processed in a three-stage programmable air furnace (Vulcan Benchtop Furnace, York, PA). The following heat treatment schedule was used for this study: de-binding at a heating rate of 0.1°C/min to 550°C; heating rate increased to 1°C/min until a final sintering temperature of 570°C with a 1 hour hold for 13-93B3 scaffolds (700°C and 1 hour hold for 13-93 scaffolds) and then the furnace was turned off and allowed to cool naturally to room temperature. Optical microscopy was used to measure the pore sizes and dimensions of the sintered scaffolds. Scaffolds measuring 1 cm x 1 cm and ~3 mm thick containing at least two rows of the lattice unit were used in the experiments so that the effect of pore geometry could be investigated. The scaffolds were ultrasonically cleaned in distilled water 3 times for 5 minutes each, followed by a similar cleaning procedure using ethyl alcohol. 13-93B3 scaffolds were only cleaned with ethyl alcohol as they are known to be highly reactive with water. The scaffolds were then dry-heat sterilized overnight at ~200°C before using them for cell proliferation tests.

2.2. Cell proliferation tests

The established MLO-A5 line of mouse late-osteoblast, early-osteocyte cells was used as a model for the *in vitro* tests to determine cell growth [20]. The cells were cultured in phenol red free α-MEM medium supplemented with 5% fetal bovine serum and 5% new born calf serum (Life Technologies, Grand Island, NY). Scaffolds were placed on a sterilized teflon sheet and seeded with 80,000 MLO-A5 cells suspended in 40 µl of complete medium. After a 2 h incubation to allow cell attachment, the scaffolds with attached cells were transferred to a 12-well plate with 2 ml of complete medium per well and incubated at 37°C in a humidified atmosphere of 5% CO_2. The media was replaced every two days during the incubation period. The cell-seeded scaffolds were placed in a medium containing the tetrazolium salt MTT (50 µg per 250 µl of medium) for the last 4 h of incubation to permit visualization of metabolically active cells. The samples were rinsed with phosphate buffered saline (PBS) at the conclusion of the incubation period and blotted dry. The insoluble purple formazan, which is the product of mitochondrial MTT metabolism, was then extracted from the scaffolds with 2.0 ml of ethyl alcohol and measured at a wavelength of 570 nm using a spectrophotometer (Evolution 300 UV-Vis, Thermo Scientific, Bannockburn, IL).

2.3. Statistical analysis

At least three samples in each set (2, 4, and 6 days) were used for cell proliferation tests, and the absorbance data collected from the spectrophotometer is reported as mean ± SD. Analysis for differences in absorbance after the incubation period and among different architectures was performed using one-way ANOVA with Tukey's post hoc test. Differences were considered significant for $P < 0.05$.

3. Results and Discussion

3.1. Design and fabrication of 13–93 and 13–93B3 scaffolds

The CAD models of the repeatable units of the five architectures considered in this work are shown in Figure 1(a). The first unit cube, termed as a "cubic" architecture, is modeled using solid tubular structures which are perpendicular to each other and running in the x, y, and z directions. The second unit cube is formed by subtracting a sphere from a solid cube and is termed as a "spherical" pore architecture based on the geometry of the pore formed in the design. The third unit cube is formed by diagonally joining the corners of a unit cube with tubular structures and is termed the "X" architecture. These three architectures could be termed as typical and frequently used designs in most of the AM techniques to manufacture scaffolds. The fourth and fifth are "diamond" and "gyroid" architectures, which are based on the freeform surface and try to mimic the trabecular architecture of bone. More about the scaffold architectures, fabrication, and their mechanical properties can be found in our previous work [14]. The fabricated scaffolds, after binder burnout and sintering, are shown in Figure 1(b) as representative specimens from each of the five architectures in the same order as shown in Figure 1(a). All the scaffolds shown in Figure 1(b) have a measured porosity of ~50%. The scaffolds were cut to about ~3 mm thick such that at least two rows of repeatable unit cells would be available to investigate the cell proliferation using the *in vitro* assessment.

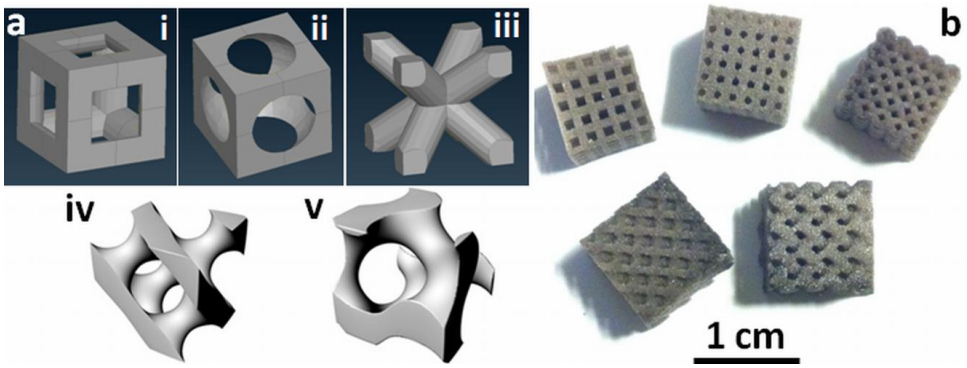

Figure 1. (a) CAD models of the repeatable units of five architectures: (i) cubic, (ii) spherical, (iii) X, (iv) diamond, and (v) gyroid; (b) 13-93B3 scaffolds with the five different architectures after sintering.

3.2. Cell proliferation on 13–93 scaffolds

Figure 2(a) shows a schematic of the static cell seeding on the scaffolds and how they are kept in a 12-well cell culture plate. At the time of cell seeding, all of the cell suspension volume applied to the scaffolds adhered to the samples since no suspension was observed on the teflon sheet after the scaffolds were aseptically transferred to the 12-well plate. Optical images of cell-seeded scaffolds with the five different architectures, and incubated with MTT during the last 4 hours of incubation for intervals of 4 and 6 days, are shown in Figure 2(b). The relative intensity of purple formazan staining on these scaffolds was found to increase with the duration of incubation. This is an indication of metabolically active cells undergoing vigorous growth on the scaffolds. The higher cell density (based on the purple color intensity) on the scaffolds with gyroid and diamond architectures in comparison to the scaffolds with cubic, spherical and X

architectures can be observed from the optical images of the scaffolds after 4 days of incubation. The scaffolds with the diamond architecture were completely covered with metabolically active cells after 6 days of incubation. To quantify the results, the measured absorbance of the amount of formazan product of mitochondrial metabolism that was recovered from the cell-seeded scaffolds labeled with MTT is plotted in Figure 3.

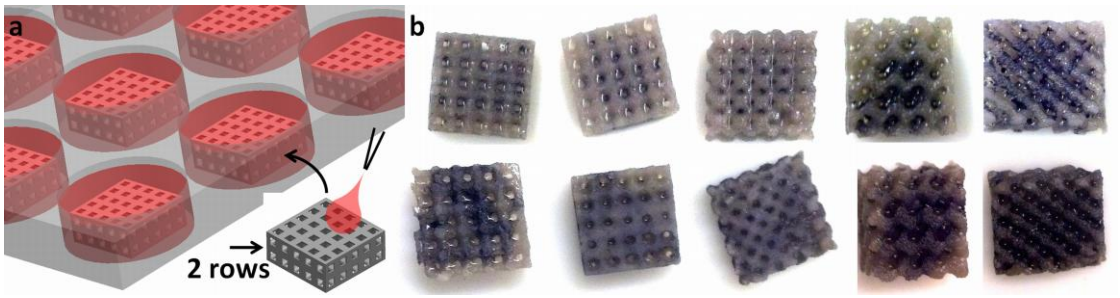

Figure 2. (a) Schematic of the static cell seeding on the scaffold with at least two rows of repeating units. The cell seeded scaffolds were later transferred to a 12-well cell culture plate, (b) Optical images showing the MTT labeling of MLO-A5 cells on the on the scaffolds (L-R: cubic, spherical, X, gyroid and diamond) after cell culture intervals of 4 days (top row) and 6 days (bottom row).

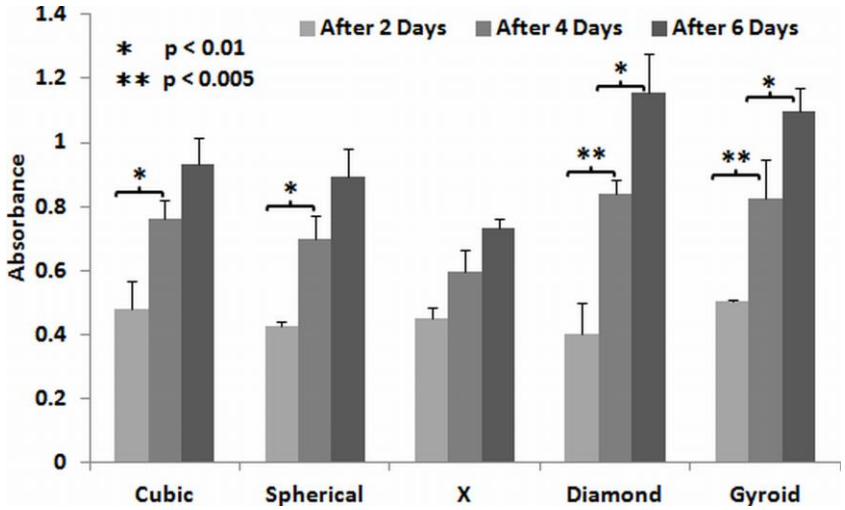

Figure 3. The absorbance values representing the measurement of cell growth plotted for all the scaffolds after 2, 4, and 6 days of incubation. Diamond and gyroid architectures show better overall cell proliferation compared to the other architectures.

The absorbance values plotted in Figure 3 for different scaffolds after 2, 4, and 6 days of incubation indicate the number of metabolically active cells on the scaffold, thereby directly corresponding to the amount of cell proliferation. To understand the cell proliferation trends from 2 to 4 days, it can be observed from Figure 3 that all the scaffolds provide significant cell proliferation except the scaffold with the X architecture. Further, the diamond and gyroid scaffolds show higher significance ($p < 0.005$) in comparison to the cubic and spherical scaffolds. Whereas the cell proliferation from 4 to 6 days was significant for the gyroid and diamond architecture scaffolds ($p < 0.01$), the increase in cell proliferation for the other scaffolds was not significant. These results indicate that although the cubic and spherical scaffolds provide

significant growth up to 4 days, the gyroid and diamond scaffolds provide significant growth up to 6 days of incubation, and the scaffold designed with the X architecture provides the least amount of cell growth. To interpret the results among the scaffolds with different architectures based on their incubation period, no significant difference was noticed after 2 days of incubation as the scaffolds have similar values of absorbance. However, the differences were observed after 4 and 6 days of incubation. After 4 days of incubation, the scaffolds having the diamond and gyroid architectures offered significantly higher cell proliferation ($p < 0.05$) in comparison to the X scaffolds. However, this difference was not significant in comparison to the cubic and spherical scaffolds. After 6 days of incubation, the cell proliferation on the diamond and gyroid scaffolds further improved in significance in comparison to the X scaffolds (from $p < 0.05$ after 4 days to $p < 0.005$ after 6 days). Also, the cell proliferation on the diamond scaffolds was significantly higher than the cubic and spherical scaffolds (with no significant difference among them after 4 days, changing to significant with $p < 0.05$ after 6 days).

3.2. Cell proliferation on 13–93B3 scaffolds

The average absorbance value of the formazan extracted after 2 days of incubation from the 13-93B3 scaffolds was ~0.3 without any significant difference among the scaffolds with different architectures. In comparison, the absorbance values representing the cell growth on 13-93 scaffolds after 2 days was ~0.4 (Figure 3). The cell proliferation results on the 13-93B3 scaffolds indicate that the amount of formazan recovered from the scaffolds after 4 and 6 days of incubation is decreasing, which is in sharp contrast to the result observed with the 13-93 scaffolds. Figure 4 shows the comparison of the absorbance values of the formazan product recovered from 13-93 and 13-93B3 scaffolds. The absorbance values in almost all the cases after 4 and 6 days were measured to be ~0.2 or less, which is too low for the result to be significant.

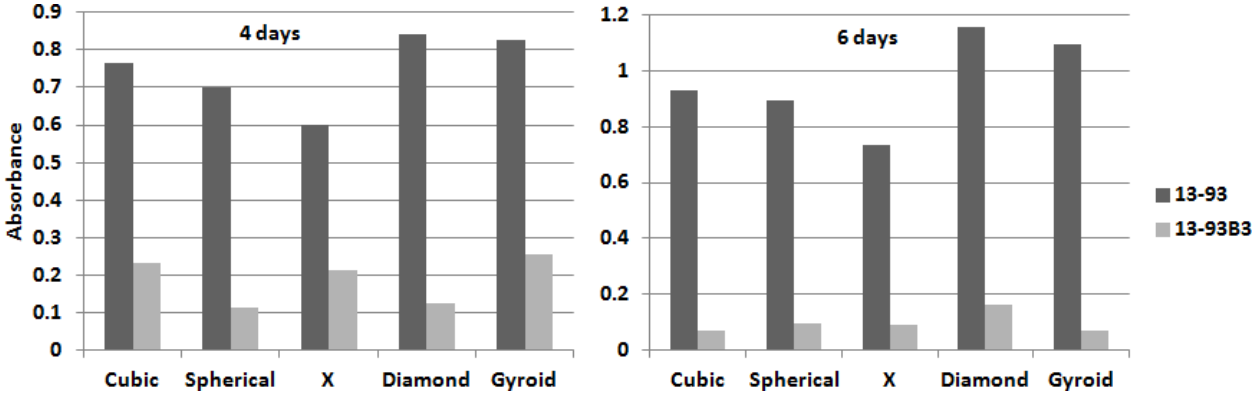

Figure 4. Comparison of the absorbance values for 13-93 and 13-93B3 scaffolds after 4 and 6 days of incubation. The graphs indicate the reduced number of metabolically active cells on the 13-93B3 scaffolds compared to the 13-93 scaffolds.

The results of *in vitro* assessment of borate based glasses reported in the literature are mixed. There have been some reports on the cytocompatibilty of the borate glass and the osteogenic differentiation of the human mesenchymal stem cells [21]. There have been other studies which reported a reduction in the absorbance value with an increase in the boron ion concentration in the cell culture media [22]. The reduction of metabolically active cells after 4 and 6 days in our study (Figure 4) may be due to the fact that an increase in the boron ion

concentration leads to an increase in the pH value of the culture media (pH – 9). Such an environment could drastically affect the growth of cells. It should be noted that this result was observed even after replacing the media every day for the 13-93B3 scaffolds in order to reduce the likelihood of a change in pH. In comparison, the media for 13-93 scaffolds was replaced every other day. Though the *in vitro* assessment of the 13–93B3 scaffolds showed poor cell survival rates, because of the toxicity attributed to boron ion release and its concentration, the results could be regarded as a false negative based on the *in vivo* assessment of the borate glasses which has been shown to demonstrate markedly faster bone growth and healing, as reported in the literature [7]. In fact, borate glasses have also been shown to even promote angiogenesis and healing in difficult-to-treat soft tissue wounds in diabetic patients [7]. The investigation of the effect of pore geometries in bone growth using the 13–93B3 scaffolds *in vivo* will be a subject of our future work.

3.3. Effect of pore geometry on cell proliferation

Apart from the differences in the cell proliferation based on the material used to fabricate the scaffolds, the surface roughness of the scaffold, which is a characteristic of the SLS process and is irrespective of the geometry, could also affect the way cells proliferate on the scaffolds. Our *in vitro* assessment results indicated that during the initial 2 days of incubation, the difference in the amount of cell proliferation among the scaffolds with different pore geometries did not exist and became significant only after 4 and 6 days. This could be due to the rough surface of all of the scaffolds fabricated by the SLS process. Figure 5a shows a scanning electron microscopy (SEM) image of a strut with rough edges due to the layer-by-layer fabrication process. Another SEM image of the surface area surrounding a pore on the scaffold, irrespective of the material and scaffold pore geometry, is shown in Figure 5b. This amount of surface roughness could provide a favorable attachment surface for seeded cells on SLS-based scaffolds. In fact, at the time of cell seeding, all of the cell suspension volume applied to the scaffolds adhered to the samples and no suspension was observed on the teflon sheet after the scaffolds were aseptically transferred to the 12-well plate (100% seeding efficiency). Therefore, during the initial days of incubation, the cells would proliferate on the rough surface of the scaffold as shown in the schematic in Figure 5c. This could be the reason for not having any significant differences among the different architectures after seeding all the scaffolds with equal number of cells and 100% seeding efficiency. The effects of pore geometry would start to prevail only after the rough surface is covered by the cells, i.e., after 4 and 6 days.

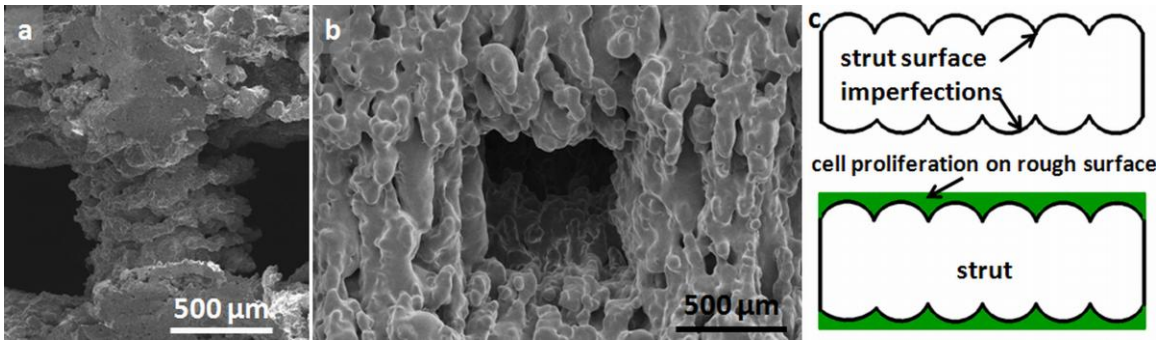

Figure 5. (a) The surface of the strut exhibiting layered fabrication in the SLS process, (b) a typical surface of the SLS scaffold, (c) schematic showing the proliferation of cells on the rough surface during the initial incubation period.

The effect of pore geometry on tissue growth and the biochemical signals between cells, as well as how the cells react to the radius of curvature of the scaffold, is still a subject of investigation to the scientific community [15, 23, 24]. While some studies have reported that tissue growth relates to curvature, other studies found no effect of curvature on tissue growth; and most of the studies are speculative in nature. In order to comprehend the differences in cell proliferation among the scaffolds in this study, the internal surface area per unit volume was calculated for the scaffolds with different pore geometries, based on their CAD files, since a higher surface area translates to more area for cells to proliferate on the surface. The value for the X architecture (0.7 mm^{-1}) was much lower in comparison to the other architectures (1.4 for cubic, 1.9 for gyroid, and 1.5 for spherical and diamond), and it reflects in the cell proliferation results as the X scaffold offered no significant cell growth (Figure 3). However, the internal surface area per volume alone does not explain the differences in the cell proliferation among the scaffolds. Though the scaffolds with spherical and diamond architecture have the same value of internal surface area per volume, the cell proliferation results are in sharp contrast in that the cells seeded on the scaffolds with the diamond architecture proliferate significantly more in comparison to the spherical scaffolds. Therefore, the perimeter of a unit cell is plotted with respect to the thickness (height) of the unit cell to understand the changes in the surface area of a unit cell rather than the overall value. Figure 6 shows the variation in the perimeter of the cross section of a unit cell along the thickness, for all the five architectures. As the length of unit cell is not uniform among the different architectures, the z height is divided by the unit cell length to provide the z value, which varies from 0 to 1 corresponding to the start and finish of the unit cell thickness. Similarly, the perimeter values are also converted to ratios based on the maximum perimeter value for the corresponding unit cell. The curvature of the internal surface could be understood from the variation of the perimeter of the unit cell for different architectures. Among all the scaffolds, the perimeter profile of the diamond architecture resembles a trigonometrical function (sine/cosine) with more frequent changes in sign (positive to negative and vice versa) to the slope of the curve whereas the changes to the slope of the curve are not drastic for the spherical architecture. Such frequent and drastic changes to the slope of the perimeter profile suggest a larger curvature to the unit cell, which offers a higher cell proliferation as observed from our results (Figure 3). A relatively slow change in slope or a constant slope of the perimeter profile would suggest small or no curvature which appears to be less beneficial for cell proliferation, especially in a static cell culture condition where the nutrient flow is limited and the only external stimulus for the cells to proliferate could be the curvature. In the case of diamond and gyroid architectures, a larger surface area, together with a larger surface curvature, might allow for better cell proliferation in the static cell culture conditions. Therefore, it can be stated that a preferable porous scaffold for tissue engineering applications should provide the necessary surface roughness for the initial cell attachment, and a larger surface area and surface curvature for improved cell proliferation.

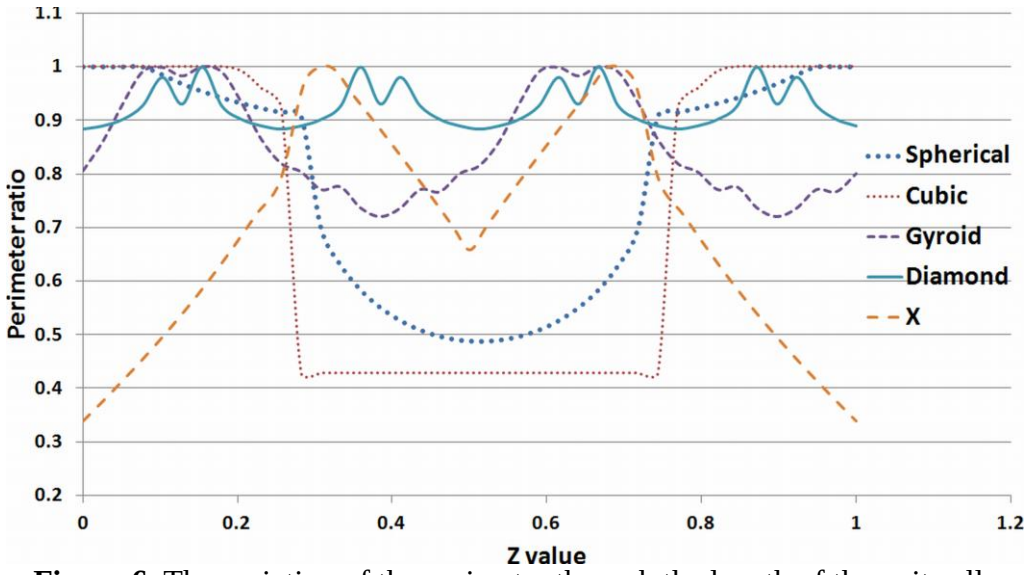

Figure 6. The variation of the perimeter through the length of the unit cell.

4. Conclusions

The *in vitro* assessment in this study indicates that bioactive glass scaffolds fabricated by the selective laser sintering process provides the necessary surface roughness for the initial phase of incubation for cell attachment. The cell proliferation study shows the effectiveness of SLS produced, gyroid and diamond architectures in providing sustained cell proliferation for 6 days of incubation compared to other scaffold architectures (cubic, spherical, and X architectures) which did not provide significant cell growth after 4 days of incubation. Our experimental results and analysis indicate that a larger surface area per unit volume of the scaffold, combined with a larger surface curvature, allows for improved cell proliferation *in vitro* for the scaffold architecture.

References

[1] Hench, L.L., Wilson, J., An Introduction to Bioceramics (Singapore: World Scientific Publishing Co. Pte. Ltd.) p 47 (1993).

[2] Hench, L.L., The story of bioglass. *J Mater Sci: Mater Med.* 17, 967–978 (2006).

[3] Rahaman, M.N., Day, D.E., Bal, B.S., Fu, Q., Jung, S.B., Bonewald, L.F., Bioactive Glass in Tissue Engineering. *Acta Biomater.* 7, 2355-2373 (2011).

[4] Liu, X., Rahaman, M.N., Fu, Q., Bone regeneration in strong porous bioactive glass (13-93) scaffolds with an oriented microstructure implanted in rat calvarial defects. *Acta Biomater.* 9, 4889-4898 (2013).

[5] Brown, R.F., Day, D.E., Day, T.E., Jung, S., Rahaman, M., Fu, Q., Growth and differentiation of osteoblastic cells on 13–93 bioactive glass fibers and scaffolds. *Acta Biomater. 4*, 387-396 (2008).

[6] Velez, M., Jung, S., Kolan, K.C.R., Leu, M.C., Day, D.E., Chu, T-M.G., In-vivo evaluation of 13-93 bioactive glass scaffolds made by selective laser sintering. In

Biomaterials Science: Processing, Properties and Applications II: *Ceramic Transactions*, Vol. 237, John Wiley & Sons, Inc., NJ, USA (2012).

[7] Jung, S.B., Bioactive borate glasses. In Bio-glasses: An introduction, First edition, Eds. Jones, J., and Clare, A.G., John Wiley & Sons, Inc., NJ, USA, p 75 (2012).

[8] Doiphode, N., Huang, T., Leu, M., Rahaman, M., Day, D., Freeze extrusion fabrication of 13-93 bioactive glass scaffolds for bone repair. *J. Mater. Sci.: Mater. Med.* 22, 515-523 (2011).

[9] Liu, X., Rahaman, M., Hilmas, G., Bal, S., Mechanical properties of bioactive glass (13-93) scaffolds fabricated by robotic deposition for structural bone repair. *Acta Biomater.* 9, 7025-7034 (2013).

[10] Fu, Q., Saiz, E., Tomsia, A.P., Direct ink writing of highly porous and strong glass scaffolds for load-bearing bone defects repair and regeneration. *Acta Biomater.* 7, 3547-3554 (2011).

[11] Michna, S., Wu, W., Lewis, J., Concentrated hydroxyapatite inks for direct-write assembly of 3-D periodic scaffolds. *Biomaterials.* 26, 5632-5639 (2005).

[12] Kolan, K.C.R., Leu, M.C., Hilmas, G.E., Brown, R.F., Velez, M., Fabrication of 13-93 bioactive glass scaffolds for bone tissue engineering using indirect selective laser sintering. *Biofabrication.* 3, 025004 (2011).

[13] Kolan, K.C.R., Leu, M.C., Hilmas, G.E., Velez, M., Selective laser sintering of 13-93 bioactive glass. *Proc. of the 21st Annual Int. Solid Freeform Fabrication Symp. Austin, TX* 504-512 (2010).

[14] Kolan, K.C.R., Leu, M.C., Hilmas, G., Comte, T., Effect of architecture and porosity on mechanical properties of borate glass scaffolds made by selective laser sintering. *Proc. of the 24th Annual Int. Solid Freeform Fabrication Symp. Austin, TX* 816-826 (2013).

[15] Rumpler, M., Woesz, A., Dunlop, J.W.C., Dongen, J.T., Fratzl, P., The effect of geometry on three-simensional tissue growth *J. R. Soc. Interface* 5 1173-80 (2008).

[16] Mitsak, A., Kemppainen, J., Harris, M., Hollister, S., Effect of polycaprolactone scaffold permeability on bone regeneration *in vivo*. Tissue Engineering: Part A 17 1831-1839 (2011).

[17] Melchels F, Barradas A, Blitterswijk C, Boer J, Feijen J, Grijpma D, Effects of the architecture of tissue engineering scaffolds on cell seeding and culturing *Acta Biomater.* 6 4208-17 (2010).

[18] Sobral J M, Caridade S G, Sousa R A, Mano J F, Reis R L, Three-dimensional plotted scaffolds with controlled pore size gradients: Effect of scaffold geometry on mechanical performance and cell seeding efficiency. *Acta Biomater.* **7** 1009-18 (2011).

[19] Kolan, K.C.R., Leu, M.C., Hilmas, G.E., Velez, M., Effect of material, process parameters, and simulated body fluids on mechanical properties of 13-93 bioactive glass porous constructs made by selective laser sintering. *Journal of the Mechanical Behavior of Biomedical Materials.* 13, 14-24 (2012).

[20] Kato, T., Boskey, A., Spevak, L., Dallas, M., Hori, M., Bonewald, L., Establishment of an osteoid preosteocyte-like cell MLO-A5 that spontaneously mineralizes in culture *J. Bone Min. Res.* 16 1622-33 (2001).

[21] Marion, N.W., Liang, W., Liang, W., Reilly, G.C., Day, D.E., Rahaman, M.N., Mao, J.J., Borate glass supports the in vitro osteogenic differentiation of human mesenchymal stem cells. Mechanics of advanced materials and structures, 12(3) (2005).

[22] Fu, H., Fu, Q., Zhou, N., Huang, W., Rahaman, M.N., Wang, D., Liu, X., In vitro evaluation of borate-based bioactive glass scaffolds prepared by a polymer foam replication method. *Materials Science and Engineering C*, 29 (7) 2275–2281 (2009).
[23] Ripamonti U, Roden L, Renton L, Klar R and Petit J-C, The influence of geometry on bone: formation by autoinduction. *Science in Africa* (2012).
[24] Rumpler M, Woesz A, Varga F, Majubala I, Klaushofer K and Fratzl P, Three-dimensional growth behavior of osteoblasts on biomimetic hydroxylapatite scaffolds *J. Biomed. Mater. Res.* 81A 40-50 (2007).